Design of self-actuating rear wing using shape memory effect

Ishan Sharma
Graduate Student, Department of Mechanical Engineering
Clemson University

Abstract

With the growing & complex demands of the current automotive sector, there has been a constant need to improve the structure and dynamics to make them efficient. Over the years, to reduce the sprung mass, there have been consistent efforts to achieve light-weight character in a different structure to improve the overall weight dynamics. The very idea to enhance the weight dynamics, the formula one environment with its dynamic and variable requirements, to maneuver over the complex racing circuits. There has been a constant push into exploring options for developing structural components that could exhibit self-actuation. The self-actuation mechanism would most certainly remove the weight of actuators. Most certainly would provide the structure the ability to work under dynamic configurations for different operating conditions at a given instant of time. Under the presented research, a design concept of reinforcing the current wing with the usage of shape memory alloy on the external surface to actuate the wing has been explored. A comprehensive analysis of the concept using different simulations has been carried out to examine the feasibility of the concept. With the limited scope of the current research, the present study does not delve into concept validation and verification with real-time load conditions, most certainly requiring more comprehensive modeling of the impact loads and design load studies with time-dependent studies.

Introduction

The advent of globalization and the growing demand for transportation have an impact on different industries. Indeed, it has served to be a catalyst for the growth of the aerospace industry. Over the years, demands have significantly risen from other parts of the world for transportation. There have been consistent efforts to improve the overall design efficiency and improve the dynamics.

In Aerospace Industry, aerodynamics and the associated design principles have always played an essential role in defining the future trajectory of aircraft design. This specific wing of study, i.e., 'Aerodynamics,' has played a significant role in providing access to this medium of transportation to several parts of the world.

Aerodynamics is a branch of study that deals with how air flows around a given object and how it could affect its motion. It certainly explains the dynamics behind the flight and what all things are pertinent in a given design to make it 'flying ready.' Moreover, it is a study to observe the effect of the air and its behavior on a given set of dynamic motions in a given environment. Though, the term 'aerodynamics' has off-lately been replaced by '*Gas Dynamics*,' a more comprehensive study, which is engaged in

Studying the motion of all gases and is not just limited to air. The wing of 'gas dynamics has led extensive efforts to lead and research compressible flows and tabulate turbulence behavior.

Majorly, there are four different types of forces that play a significant role during a given flight are:

- *Lift Force Component:*

The force component perpendicular to the applied flow is called the lift force component. The same force component is utilized in Racecar dynamics to unleash the downforce dynamics discussed in the later sections.

- *Drag Force Component:*

The drag force component is applied parallel to the flow of fluid and often applied opposite to the direction of fluid flow, which opposes a given motion in the forward direction. In Racecar dynamics, a proper trade-off between the downforce generation and the induced drag at a given instant must be maintained in a given design for the optimal performance of the wagon. Drag force component is further categorized into – skin friction drag, induced drag and form drag.

- *Thrust Force Component:*

The thrust force components enable to overcoming the drag and keeping it moving forward in the desired direction of ascent. In some cases, the thrust forces also help in some situations of descent during different aviation operations. The vitally the

thrust force component does not play an integral role in the race car dynamics study.

- *Self-Weight Force:*

The force experienced due to the self-weight of the body/object. This force components is one of the critical components which are studied during the lightweight design aspects of race-car. Though, the lightweight engineering has now extended to be an individual branch of study to work towards developing light weight structures which could provide same level of robustness, durability and performance.

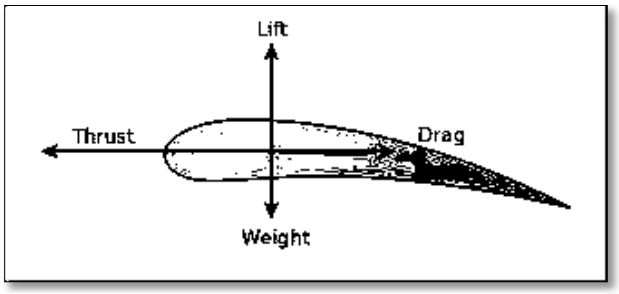

Figure 1: Force representation over an Airfoil [4]

Among the above-classified force components, the lift and the drag component are the aerodynamic forces. Calculations of these fields (Lift and Drag force components) hold only with the assumption that the flow field behaves as a '*continuum*.'

The concept of the continuum is a phenomenon of idealizing matter as space with a continuous distribution of matter that could be further divided indefinitely to study the effects. The idealization that the matter is made from individual atoms is ignored. The continuum idealization further helps to solve problems using the three fundamental laws:

- *Conservation of Mass:*

The law of conservation of mass states that the mass can be neither be created nor destroyed. In each system in reference, a mass is conserved, i.e., Incoming Mass is equivalent to the Outgoing Mass for a given system at a particular time instant.

In fluid mechanics, the law of conservation of mass is expressed using continuity expression in the differential form as shown below:

$$\frac{\partial \rho}{\partial t} + \nabla.(\rho \boldsymbol{v}) = \mathbf{0}$$

Where ρ: density (mass per unit volume), t is time (in sec),$\nabla.(\rho \boldsymbol{v})$: is the calculated divergence over density & flow velocity product (v).

- *Conservation of Energy:*

The law of conservation of energy states that for an isolated system, energy for a given system remains conserved over time. The energy for a given system can neither be created nor destroyed, though energy can be exchanged from one medium to another.

The law of conservation of energy can be expressed using differential as shown below:

$$E_{in} - E_{out} = \Delta E_{System}$$

Where the LHS, difference between E_{in} and E_{out} , Is nothing but the rate of net energy transfer. RHS of the above expression represents the rate of change of energy for a given system.

Energy Balance expression:

$$dE = \partial Q - \partial W$$

$$\frac{dE}{dt} = Q - W$$

By the first law of thermodynamics, energy enters a system only when the net heat is transferred into the control volume. If energy leaves the system, it's because control volume completes a net resultant work over the given environment/surrounding.

- *Conservation of Momentum:*

The law of conservation of momentum states that for a given system in reference, the total momentum for the system will remain conserved.

The law of conservation of momentum is integral when dealing with vector quantities, which posses' magnitude as well as the direction.

Expression for law of conservation of momentum as shown below:

$$F = m * a = m\,\frac{\Delta u}{\Delta t}$$

$$-\left[(p * A)_2 - (p * A)_1\right] = m\,\frac{u_2 - u_1}{\Delta t}$$

$$-\left[\left(p + \left(\frac{\Delta p}{\Delta x}\right)\Delta x\right)A - pA\right] = m * \frac{u + \left(\frac{\Delta u}{\Delta x}\right)\Delta x - u}{\Delta t}$$

It can be expressed in *differential form* as:

$$-\frac{dp}{dx} = \rho * u\,\frac{du}{dx}$$

Aerodynamics of cars

In Automotive Industry, with the emergence of fast-moving transportation and Following through the demand for energy-efficient vehicles, the study of aerodynamics has significantly played an essential role in the automotive industry.

Over the years, with the growing popularity of formula one, it has been a spot for all the most raging competition between OEMs to prove their prowess in the field. The field of aerodynamics has significantly evolved with motorsport. Manufacturers have been significantly interested in the generation of down-force in a fast-paced environment of formula one by utilizing wings in their design. The same principle inspires the aerospace industry and automotive industry in wing-utilization, but functional utilization is different.

In Aircraft, the lift is generated due to pressure differences on the top and bottom surface of the wing. The wing's lift is complemented by the thrust generated by the aircraft engines to propel in the desired direction. The same principle of thrust when reversed is often utilized for *'Reverse Thrust Braking*' in case of slip-off on the runway, often utilized in emergency maneuvers. This principle helps an aircraft to lift off and smoothly take off from the runway.

The working principle is reversed in the automotive industry, where the wing generates downforce, which brings much-needed traction at high-speed maneuvers. The downforce helps the vehicle maintain the contact patch with the ground during those high-speed maneuvers around the corners helping the vehicle gain the much-needed traction at tight corners. It also prevents frequent degradation of the tire, reducing frequent pit-stops for a tire change during the race.

Now, the very advantage of downforce providing the much-needed traction also comes with the disadvantage of the drag force generated due to the downforce. The downforce is proportional to the applied drag in a given maneuver, with the increase of downforce would lead to an increase in aerodynamic drag.

Vehicle Dynamics & Stability

Among the different factors which affect the performance of the car, one among them is the mechanical grip over the contact patch, often termed as 'traction'. The ideal requirement of the design is to have optimal downforce with minimalistic induced drag due to generated downforce.

In tight maneuvers of the corner at high speed, the downforce enables to maintain the control and as well as stability throughout the course of the maneuver. At the same time, the drag force leads to dissipation of usable energy/work that often reduces the capacity of the vehicle to accelerate aggressively during its motion. At the same time, wings contribute towards making the flow streamline, in that case, front wings are majorly responsible to make the flow streamline that indirectly affects the amount of applied drag at a given instant of time.

Rear wing plays a major role in ensuring that the tipping boundary layer of the aerodynamic environment remains streamlined and does not ends up creating the turbulence at the boundaries, as it would lead to creation of vortices. These vortices would eventually lead to a creation of *'upwash'* in the region, that eventually changes the ideal angle of attack for the given geometry.

Concept of Wing & Airfoil

Wing constitutes one of the most integral structural aspect in the study of aerodynamics. Primarily, wings were just meant to produce the lift enough to carry its self-weight. In Automotive sector, the wings are primary used for generating downforce, which entail would ensure adequate contact patch during a given maneuver.

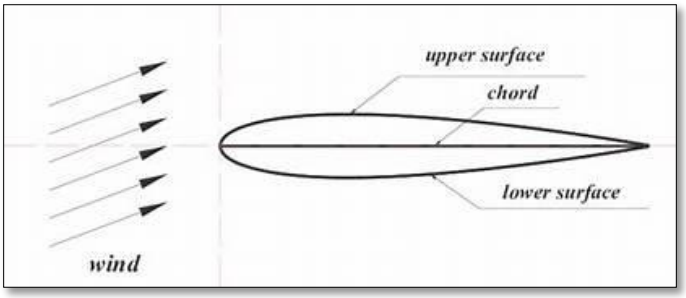

Figure 2 Wing Dynamics of Chord, Lower Surface & Upper Surface [6]

This would lead to a more stable vehicle performance and at the same time ensuring the traction is also maintained during maneuvers. The required amount of lift force for an aircraft is equivalent to the product of load factor and self-weight. The load factor value ranges from 1.05 – 1.25 for various commercial aircraft applications. In Automotive, the wing dynamics are reversed to generate the downforce, which is calculated as the minimum force required to adequately maintain contact patch with bare-minimum entailed drag.

In usual design of the wing, the low pressure, high wind velocity region is generated on the upper surface of the wing and other hand, the high pressure, low wind velocity area is generated over the lower surface of the wing. Now as the dynamics of the wings are reversed in this case, the high-pressure region is developed over the upper surface in case of automotive wings, leading to lower pressure area underneath the wing. This phenomenon helps to create the much-needed downforce.

Types of Wing

To deal and handle the aerodynamics in the overall design, different types of wings are introduced into the design. The use of wing design comes from prevalent utilization of rear wing by Ferrari in their formula one vehicle design.

Majorly, the wings are of two types – Front Wing and Rear Wing. In designs, the one third of the overall downforce is generated by the rear wing, though variable geometry configuration of rear wing allows designers to customize vehicles for a given operational environment. The wider the angle of the wing leads to reducing the potential top-speed a vehicle could achieve in a given environment.

Rear wing usually consists of two variable sets of airfoil geometries, which are further connected to the endplates across the wing geometry. The upper airfoil in the rear wing is majorly responsible to create most of the overall downforce generated by rear wing. In our current study, our focus is on the actuation mechanism of the upper airfoil.

Types of NACA Airfoil

The below picture describes different types of airfoils utilized for different design conditions and loading conditions. All the airfoil design shown below are NACA (National Advisory Committee of Aeronautics) compliant.

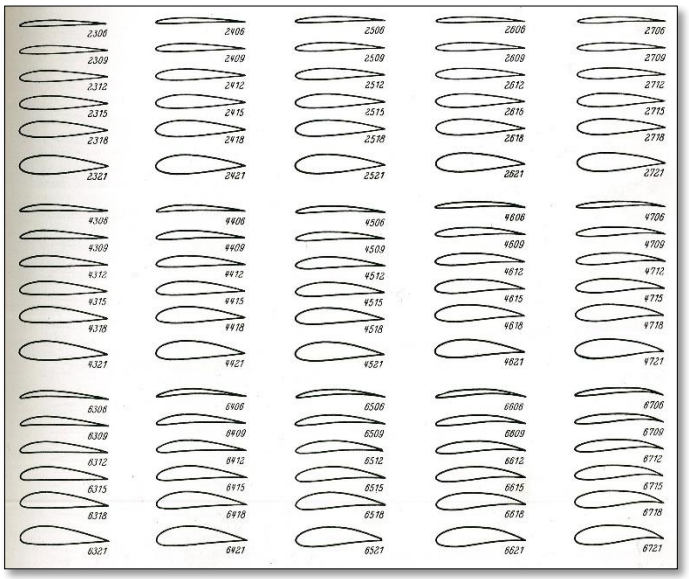

Figure 3: Different types of Airfoil geometries [3]

Concept of Morphing

Concept of morphing was initially introduced in the conceptual design studies for the aircraft to improve the overall dynamics of the aircraft structural design. It has been studied that utilizing morphing structure would not only improve the agility of the structure, to respond actively for a given stimuli. At the same time, making sure even the overall weight dynamics are also improved, which has led to improvement in overall aircraft performance.

The field of morphing is still getting developed over the years with varied research profiles to corroborate its extensive application and

Shape Memory Alloys

In recent years, with intricate and complex design demands to serve a wide array of industrial and commercial applications. There has been a consistent demand for smart materials, which possess a certain degree of control.

The desired control could be active or passive depending on the application and utilization. The demand of these materials comes from the space to reduce the overall weight dynamics to improve power to weight ratio for various applications. In transportation sector, specifically in aerospace and automotive sector, typically for actuation different type of actuators are utilized on the structure. Often the utilization of these actuators contributes towards increase the overall weight. With growing demand to improve the structure dynamics on the lines of efficiency, there has been emergent demand to make structures 'smart' enough with inbuilt self-actuating mechanism.

This had led to extensive research in the field of shape memory alloys which allow the structural researchers to delve into the realms of self-actuating structures by utilizing the shape memory effect. After observing stress-strain dynamics of shape memory alloy, it has been observed by different researchers that the shape memory alloy tends to exhibit two different type of behaviors, which does not fall under the linear response or linear behavior of the materials.

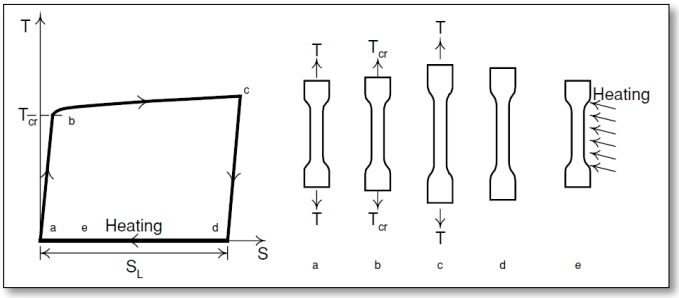

Figure 4: Shape Memory effect in shape memory material [5]

The shape memory alloy exhibits the – shape memory effect and super elastic behavior which makes it more prominent choice among different smart materials.

Applications of Shape Memory Alloys

Shape memory alloys have extensively been utilized to develop airfoils with variable geometries. These airfoils have prevalently been able to replace the conventional utilization of actuators. It also has been used in aerospace applications to decrease the turbulence over an aerodynamic surface by coupling it with MEMS device.

Among different types of available shape memory alloy's, one of the alloys created by Naval Laboratory has been actively utilized in structure these days i.e Nitinol. Nitinol comes with this unique ability to recover from large strains by undergoing phase transformation, when at a given instant stress or heat is introduced to the Nitinol.

In each condition of High Temperature, without application of any stress in each system, the Nitinol exist in austenite phase whereas when the temperature of a given system is reduced the Nitinol exists in martensite (hard & brittle state of matter) phase. Nitinol exhibits pseudo-elasticity behavior during its austenitic phase.

In a given system, when there is no stress applied at a given instant in the environment, transition between austenitic and martensitic is characterized by four transition temperatures.
A_s, A_f : Transition temperature that represents transformation from martensite to austenite phase
M_s, M_f: Transition temperature that represents transformation from austenite to martensite phase
s and f in the subscript represent the start and the finish temperature, respectively. All the four-transition temperature, follows the expression:

$$M_f < M_s < A_s < A_f$$

The observed phenomenon of shape memory effect in SMA alloys is nothing but the transformation between martensite and austenite phase, where the transformation is a function of stress and temperature.

Souza-Aurrichio Modelling Approach

Souza Aurrichio modelling approach is one of the simpler approaches to model the shape memory effect for shape memory alloys. Though, the approach has been effective to address and simulate the behavior of shape memory alloy in 3D environment.

Some of the popular inbound commercial software packages are based on Aurrichio model. They are part of the preset module of the Ansys Commercial package to simulate the shape memory effect.

Physical Properties of Nitinol (based on Aurrichio Model)		
1	Density	6.46 x 10^{-6} kg/mm3
2	Young's Modulus	80 GPa
3	Poisson's Ratio	0.35-0.43
4	Bulk Modulus	1.904 X 10^5 MPa
5	Hardening Parameter	3000 MPa
6	Reference Temperature	70 ^oC
7	Elastic Limit	120 MPa
8	Temperature Scaling Parameter	5 MPa C^{-1}
9	Maximum Transformation Strain	0.06 mm/mm $^{-1}$
10	Martensite Modulus	30,000 MPa
11	Lode Dependency Parameter	0.15
12	Ultimate Tensile Strength	754 – 960 MPa
13	Yield Strength (low temperature)	100 MPa
14	Elastic Modulus (High Temperature)	75 GPa
15	Elastic Modulus (Low Temperature)	28 GPa

Table 1: Different properties of Nitinol

Different Modelling approaches for shape memory alloys could be used to model the shape memory effect. In the further section, single variable (1D) modelling and then followed by multi-variant modelling aspects using the Brinson model has been discussed. Furthermore, the shape memory alloys can be either by modelled using 2-phase approach or three phase approach. In the further sections, only 2-phase model is considered as the basis to lead further detailed discussions.

Some of the methods referred for modelling the aspects of the given project are:

Tanaka Model

Under this model, it was proposed as one-dimensional martensite phase transformation model. Though this model's utilization scope is limited to stress-induced martensite phase-based transformation only.

As per the tanaka model, the entire thermomechanical model is one unilateral function of strain, temperature, and martensite volume fraction. Whereas the material constants also known as stress-influence coefficients, C_A and C_M are deduced from experimental findings, while working with shape memory alloy.

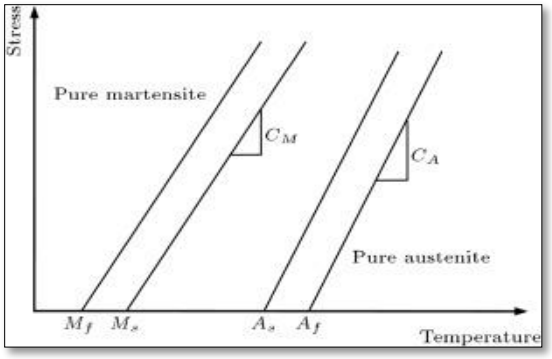

Figure 5: Stress vs Temperature plot (Tanaka Model) [2]

Constitutive Equations based on the Tanaka Model

The model possesses state variables: stress, strain and temperature, which is expressed in terms of martensite volume fraction.

$$\sigma - \sigma_O = E(\xi)(\in - \in_O) + \Omega(\xi)(\xi - \xi_O) + \theta(T - T_O)$$

Where, $(\sigma_O, \in_O, \xi_O, T_O)$ are representative of the initial state the material at the time (t = 0 sec)

$E(\xi) = E_A + (\xi)(E_A + E_M)$

Ω : Phase Transformation Coefficient

$$\Omega(\xi) = -\in_L E(\xi)$$

Where $\in_L$ represents the amount of maximum recoverable strain from a given material.

Kinetics involved in Martensite Volume Fraction:

$\xi_{A\to M} = 1 - \exp(\alpha_M(M_s - T) + b_M\sigma)$

The above expression involves representation of the martensite volume fraction

If T (reference Temperature) more than the M_f $(T > M_f)$:

$C_M(T - M_S) < \sigma < C_M(T - M_f)$

$\xi_{M\to A} = 1 - \exp(\alpha_A(A_s - T) + b_A\sigma)$

If T > A_s:

$C_A(T - A_f) < \sigma < C_A(T - A_S)$

Liang and Rogers Model:

The liang and rogers' model is similar to the tanaka model and its also utilized one dimensional constitutive modelling of shape memory alloys. Though the expression of phase kinetics is a little different when compared to the Tanaka model.

In the phase kinetics model, the cosine expression is used to express the martensite volume fraction as a function of stress and temperature.

Constitutive Modelling based on Liang and Rogers Model:

$$\xi_{A\to M} = \frac{(1-\xi_A)}{2}\cos[(\alpha_M(M_s - T) + b_M\sigma)] + \frac{(1+\xi_A)}{2}$$

For T (Reference Temperature) > M_f :

$C_M(T - M_S) < \sigma < C_M(T - M_f)$

$$\xi_{M\to A} = \frac{\xi_M}{2} * \cos[(\alpha_A(T - A_S) + b_A * \sigma) + 1]$$

For T > A_s:

$C_A(T - A_f) < \sigma < C_A(T - A_s)$

Where, material constants:

$$\alpha_A = \frac{\pi}{(A_f - A_s)}, b_A = \frac{\alpha_A}{C_A}, \alpha_M = \frac{\pi}{(M_S - M_f)}, b_M = -\frac{\alpha_M}{C_M}$$

Where ξ_M and ξ_A are the initial martensite volume fractions, prior to any of the transformations taken over the materials and its boundary conditions.

Brinson Model

As the first two models, failed to explain the shape memory effect at low temperatures, which is moreover caused due to transformation between stress-induced martensite and temperature induced martensite.

The above discussed model (Tanaka & Liang-Rogers) cannot explain the detwinning behavior of martensite, which is responsible for the shape memory effect. This model rightly addresses the short coming for the same by diving the total martensite volume fraction as a sum of stress induced component and temperature induced component.

Constitutive Modelling based on Brinson Model:

Total Martensite Volume fraction = Stress-induced component + Temperature induced component

$$\xi = \xi_S + \xi_T$$

Where,

ξ: Total Martensite Volume Fraction

ξ_S: Total Martensite Volume Fraction (Stress induced component)

ξ_T: Total Martensite Volume Fraction (Temperature induced component)

$\sigma - \sigma_O = E(\xi) * \varepsilon - E(\xi_O)\varepsilon_O - \Omega * (\xi_O) * (\xi_{s0}) + \Omega * (\xi) * (\xi_S) + \theta(T - T_O)$

$\sigma = E(\xi) * (\varepsilon - \varepsilon_L * \xi_S) + \theta(T - T_O)$

Conversion to detwinned martensite

for T > M_s &

$$[\alpha_s^{cr} + C_M(T - M_S)] < \sigma < [\sigma_f^{cr} + C_M(T - M_s)]$$

$$\xi_s = \frac{1-\xi_{s0}}{2}\cos\left[\left[\frac{\pi}{\sigma_s^{cr} - \sigma_f^{cr}}\right] * [\sigma - \sigma_f^{cr} - C_M(T - M_s)]\right] + \frac{1+\xi_{s0}}{2}$$

$$\xi_T = \xi_{TO} - \frac{\xi_{TO}}{1-\xi_{s0}}(\xi_S - \xi_{sO})$$

For T < M_s & $[\alpha_s^{cr} < \sigma < \sigma_f^{cr}]$

$$\xi_s = \frac{1-\xi_{s0}}{2}\cos\left[\left[\frac{\pi}{\sigma_s^{cr} - \sigma_f^{cr}}\right] * [\sigma - \sigma_f^{cr}]\right] + \frac{1+\xi_{s0}}{2}$$

$$\xi_T = \xi_{TO} - \frac{\xi_{TO}}{1-\xi_{s0}}(\xi_S - \xi_{sO}) + \Delta_{T\epsilon}$$

Where, if $M_f < T < M_S$ *and* $T < T_O$

$$\Delta_{T\epsilon} = \frac{1 - \xi_{T0}}{2}\{\cos[\alpha_m(T - M_f)] + 1\}$$

Else,

$$\Delta_{T\epsilon} = 0$$

Conversion to austenite:

For T > A_s and $C_A(T - A_f) < \sigma < C_A(T - A_s)$

$$\xi = \frac{\xi_0}{2}\{\cos\left[\alpha_A\left(T - A_s - \frac{\sigma}{C_A}\right)\right] + 1\}$$

$$\xi_s = \xi_{so} - \frac{\xi_{so}}{\xi_o}(\xi_o - \xi)$$

$$\xi_T = \xi_{T0} - \frac{\xi_{T0}}{\xi_o}(\xi_o - \xi)$$

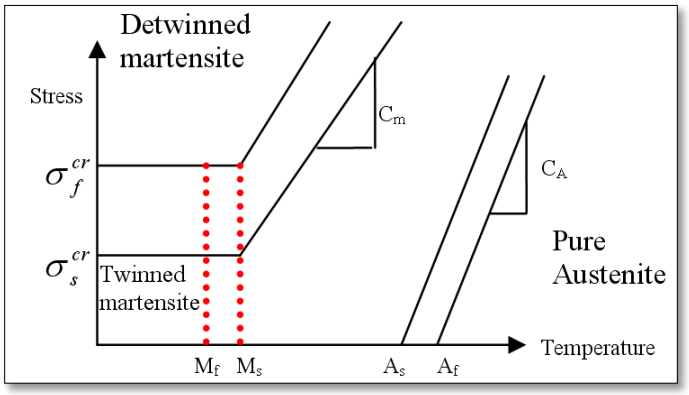

Figure 6: Temperature Vs Critical Stress plot (Brinson Model)

Correction to Brinson Modelling Approach

The original Brinson model leads to a mathematical fallacy in terms of leading the martensite volume fraction expression tends to the infinity that somehow restricts the former Brinson model to be utilized for specific initial conditions only. Regions where, the initial Brinson model fails are:

Case I: When, stress: fixed, temperature: decreases

Case II: When, temperature: decreases, stress increases simultaneously.

Modified Expression:
Case I: When $T < M_s$ *and* $\sigma_s^{cr} < \sigma < \sigma_f^{cr}$

$$\xi_s = \frac{1-\xi_{s0}}{2}\cos\left[\left[\frac{\pi}{\sigma_s^{cr} - \sigma_f^{cr}}\right] * [\sigma - \sigma_f^{cr}]\right] + \frac{1+\xi_{s0}}{2}$$

$$\xi_T = \Delta_{T\epsilon} - \frac{\Delta_{T\epsilon}}{1 - \xi_{s0}}(\xi_s - \xi_{s0})$$

Case II: If $M_f < T < M_s$ *and* $T < T_O$

$$\Delta_{T\epsilon} = \frac{1 - \xi_{T0} - \xi_{s0}}{2}\{\cos[\alpha_m(T - M_f)]\} + \frac{1 - \xi_{T0} + \xi_{s0}}{2}$$

Else,

$$\Delta_{T\epsilon} = \xi_{T0}$$

Comparison of different modelling approach

After discussing four different modelling approach, it's quite evident that two models – Tanaka & Liang-Rogers model is not capable to predict the shape memory effect in shape memory alloys. Though, all the models are able to simulate pseudo-elastic/super elastic behavior of the shape memory alloy quite accurately at high temperature environment profile.
As discussed in the improved Brinson model that the former model was inconsistent with some of the conditions and the former model holds good for some specific operational environment, which was readily addressed in the corrective kinetics model.

All the models have been graphically plotted along with the experimental data as shown in figure 7, which is a clear benchmark to analyze the accuracy of prediction. It's quite evident that Brinson model is highly accurate and the model with corrective kinetics is able to simulate real-time behavior and performance to quite an extent.

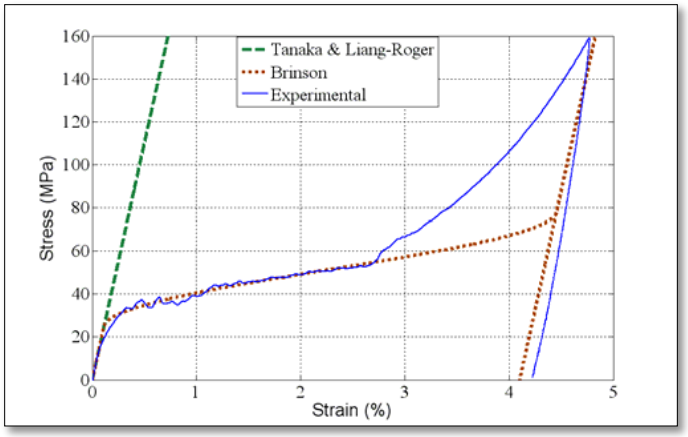

Figure 7 Stress-Strain curve plotted for different modelling approach's [2]

Project Approach

In the given project study for the rear wing design, an initial design of the rear wing is created using the parametric surfaces in the CAD environment. After the initial design for the given dimensions of rally car, the design concepts which could inhibit self-actuating character has been explored and discussed in the further sections.

Initial Design

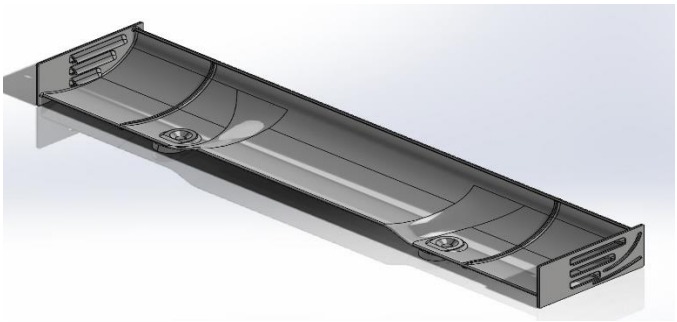

Figure 8: Initial Geometry of the Rear Wing profile (Isometric View)

Figure 9: Initial Geometry of the preliminary design (Side Profile)

Governing Equations of Deformation

Improvised Design

In the improvised design, in the direction to instill the elements of self-actuation, the wing design has been conceptualized and two of the conceptualized concepts have been discussed in the further sections. In the conceptualization stages, different options, controlled strain recovery and uncontrolled strain recovery models have been also studies.

Effort has been to develop a design concept which could lie in the controlled strain recovery paradigm and at the same time could exhibit actuation using SMA effect with approximated real-time loads.

After the discussion of the concepts, one of the concepts is further selected to lead the further research investigation.

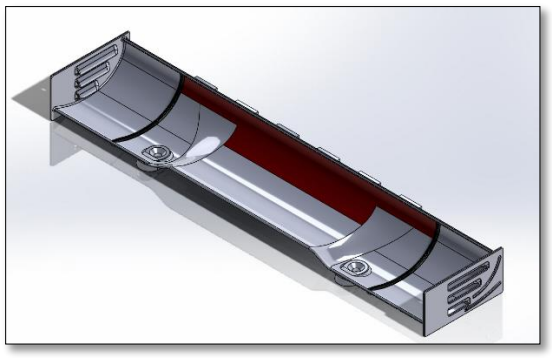

Figure 10: Improvised Design of the Rear Wing (Highlighted face in-reference for improvisation)

(Rendering Interface – Solidworks 2020)

Design Variables & Design Equations

Wing Dimension		(in mm)
1	Chord Length	14.92
2	Length of Wingspan	856
3	Reference Airfoil Profile	NACA 0012, NACA 4606

Table 2: Wing dimensions

In the series of attempts to work through different design iteration, two different concepts to improvise the design of current wing have been explored.

In the first concept, the emphasis has been onto removing the external actuation mechanism in the direction to ingrain the actuation character in the wing itself.

Concept A: of Replacing Actuators using SMA

Figure 11 Wing reinforced with SMA Actuators (Black)

In the first concept, the wing is reinforced with small SMA wedges along the length of the wing geometry. The black rendered objects as shown in the above sketch is the representation of the above concept.

The above concept has been extensively studied in the later sections of the study with different analytical & qualitative research studies to draw its working principles.

On the lines of validation, concept with such intricate geometries would need physical wind tunnel testing to gauge the limits of conceivability of the above concept. As of now, the flow obstructions which occur during the course of maneuver have been not considered under this research.

Concept B: Reinforced Sandwiched Skeleton-Skin out of Shape Memory Alloy

In this concept, the shape memory alloy is explored as a part of the reinforced sandwiched structure, which sandwiches skin and skeleton.

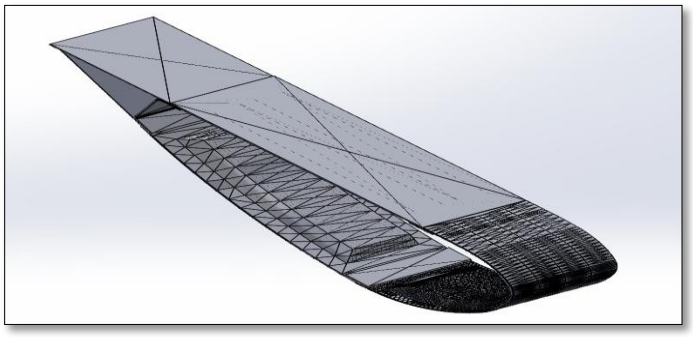

Figure 12 Internally SMA reinforced skeleton of Morphing Skin

(Rendering Interface – Solidworks 2020)

Wherein the torsion actuators (I Sections) are put between the skeleton and the skin. They are majorly responsible to control the control volume of the air and the angle of attach as to how would the air approach the geometry and could be changed as in the case of regular flapping mechanism. Though the regular flapping mechanism utilizes external actuators to achieve the objective.

Concept A is further studied and analyzed under different simulation schemes using different mathematical modelling techniques.

Morphing Skin

In the scope of this project, the torsional stiffness of the wing design is taken as constant, which varies along different plane geometries.

Though, the real time load conditions would lead to variable torsional loading conditions along the surface of the skin which would also vary at different time instants and the external environment.

Wing Design Hand Calculations

Velocity Profile		
(i)	v1	44.4 m/s / 160 kmph
(ii)	v2	80.2 m/s / 288 kmph
(iii)	v3	105.5 m/s /379.8 kmph

Table 3: Velocity Profile

Frontal Area Profile (for CFD – Wind Tunnel Simulation)	
Length	3.25 m
Width	2 m
Total Frontal Area/Draft Area (Area = Length * Width)	6.5 m^2 / 6,500,000 mm^2

Table 4: Frontal Area dimensions

Lift Force Profile			
(i)	v1	C_l = 1.01	Lift Force (L1) = 9674.128 N
(ii)	v2	C_l = 1.01	Lift Force (L2) = 31,406.96 N
(iii)	v3	C_l = 1.01	Lift Force (L3) = 54,103.2 N

Table 5: Lift Force calculations

Drag Force Profile (Includes only induced drag* - single element wing)			
(i)	v1	C_d= 0.02	Drag Force (D1) = 147.48 N
(ii)	v2	C_d= 0.02	Drag Force (D2) = 478.982 N
(iii)	v3	C_d= 0.02	Drag Force (D3) = 832.9 N

Table 6: Drag force calculations

Results & Conclusion

Pre-Processing Approach

The below picture shows the fluid structural coupling environment in the Ansys Workbench 2020R1 wherein the results observed in fluid solver are translated as input to the static structural study for the reference geometry.

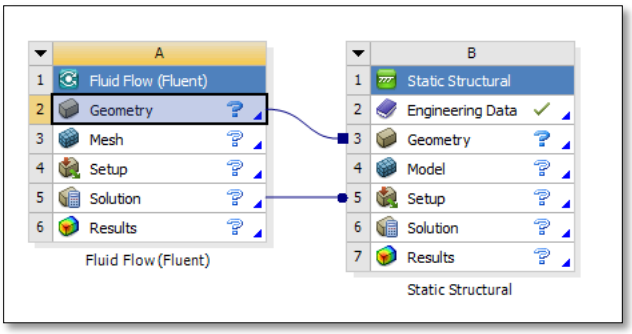

Figure 13 Setting up the fluid structural interaction

Software: Ansys Workbench 2020R1

Meshed Model

The improvised design model is meshed using program-controlled mesh with the specified quality metrics of span angle and skewness to capture geometry accurately. At the same time, avoiding mirror nodes in the given geometry.

Different layers of inflation are laid across the curved boundaries to effectively capture the curvature in the geometry.

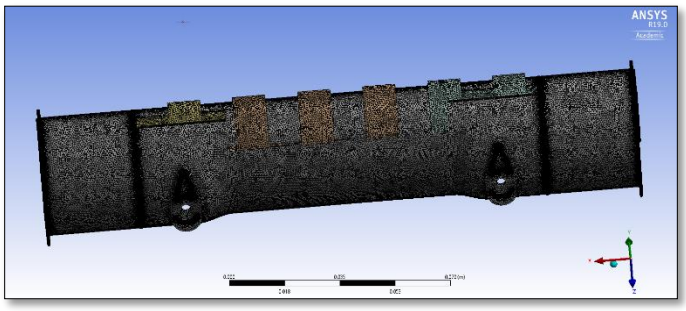

Figure 14: Meshed Model: Combination of Program Controlled & User-defined quality metrics

Solver: Mechanical Multiphysics

Computation Fluid Dynamics Study using fluid structural scheme

Using the computational fluid dynamics solver – Fluent and Mechanical Static Structural solver were coupled to conduct the design analysis.

In the analysis, the directional deformation was observed for different angle of attacks. At a given angle of attack, the coefficient of drag and coefficient of lift was derived. The optimal angle of attack and its corresponding coefficient of drag and coefficient of lift was chosen for further design analysis.

In next sections, the boundary conditions of the fluid structural coupling have been introduced to deduce coefficient of drag and lift are deduced to calculate the lift force and drag force for the given wing geometry.

Boundary Conditions

The table below captures all the conditions mandatory to fully define the problem in the fluent solver interface.

Solver		Ansys Fluent Flow
1	Inlet Conditions	Velocity field
2	Initial Velocity ($V_{initial}$)	44.4 m/s, 80 m/s, 105.5m/s
3	Approach	Dynamic Mesh – Control Volume Approach
4	Angle of Attack	Parametrized constraint (0,5,10,15,20,25,30)
5	Temperature	300.15K
6	Modelling (Wing Surface & Wingtip)	Modelled as Wall
7	Scheme utilized	Turbulent & Transitional fluid flow
8	Frontal-Area/Air Draft	6,500,000 m^2
9	NACA Airfoil	NACA 0012 inverted wing

Table 7: Boundary Conditions for Fluid Structural Scheme

Results:

In the results section, to our further research on the given rear wing only the deformation along the y-z plane holds importance rest others can be avoided due to limited scope of the current study. Some of effects pertaining to other planes have been omitted for the current scope of research.

The direction deformation results in the x, y and z direction are shown below respectively.

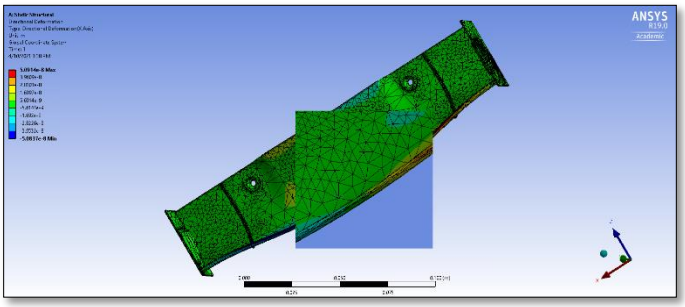

Figure 15 : Direction Deformation along x-axis (CFD Preprocessing elements suppressed)

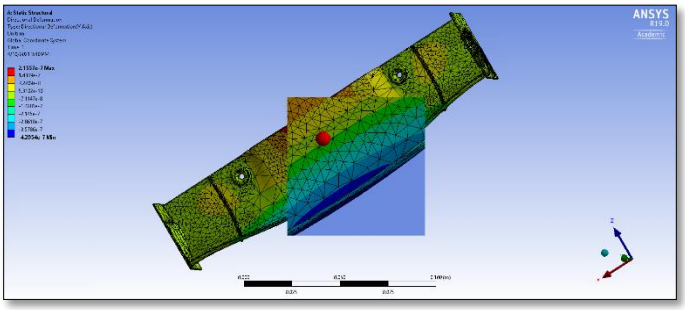

Figure 16 Direction Deformation along y-axis (CFD Preprocessing elements suppressed)

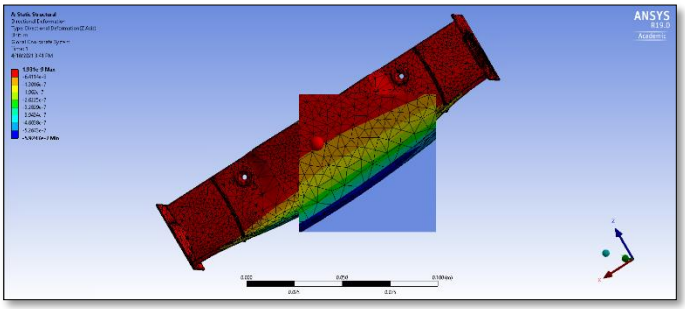

Figure 17 Direction Deformation along z-axis

Solver: CFD Fluent Linear fluid low & Static Structural Coupling (CFD Preprocessing elements suppressed)

Inferences:

After the comprehensive computational fluid dynamics study over the designed wing geometry, a parametric study was carried out with variable as angle of attack.

In experimental tests by different researchers, it was observed for different angle of attacks, it was observed, if the angle of

attack is more than 15 degree would lead to large drag force leading to decreased efficiency of the design.

Whereas on the other hand, angle of attack equal to and less than 15 degree (positive) would provide you with limited drag and optimal downforce. By utilizing the experimental findings, the parametric study in reference to the angle of attack was carried out in the periphery of 15 degree (positive).

Different angle of attack studied at five instants (0,5,10,15,20) respectively.

	Angle of Attack	*Coefficient of Drag (C_d)*	*Coefficient of Lift (C_l)*
1	*0^O*	*0.008*	*0.263*
2	*5^O*	*0.008*	*0.857*
3	*10^O*	*0.013*	*1.309*
4	*15^O*	*0.022*	*1.495*
5	*20^O*	*0.036*	*1.409*

Table 8: Coefficient of Drag & Coefficient of Lift calculated at a given angle of attack

In the CFD study, only the positive angle of attack was considered due to geometrical constraints of the design. After observing coefficient of drag and lift at different instants, angle of attack = 15 degree (positive) was chosen for the further research.

Though, with increased modularity of the design leading the current design to a modular design, then even negative angle of attack can also be explored as a future scope for the study.

Shape Memory Effect Analysis

Modelling Approach

As with limited node profiles due to academic license, the entire actuator profile has been modelled as a wedge, meshed using shell elements with preset shape memory effect module of COMSOL Multiphysics software package. The thermal-structural interaction scheme has been setup using the above discussed parameters.

The Fluid structural scheme would serve as the leading input to gauge the needed deformation for the wing to move in the desired direction. The FSI scheme has also helped and enabled to select the appropriate values of voltage and current modules for the design.

The analysis has been carried out in the quasi-static profile, which does not allow us to model the real-time impact loads (if any). The analysis section does not claims to corroborate the dynamic loads, which a wing might observe during the real time conditions.

Boundary Conditions

The boundary conditions for setting up the simulation is a mixture of data from different research articles and investigations carried out by different researchers in the past.

Whereas some of the components of experimental testing would serve as the validation to the behavior and response of the analysis. In this case, DSC experimental test data referenced from articles have been utilized to model shape memory effect.

Two different types of wedge bars have been used to lead the simulation.

Wedge Bar Dimensions

Wedge Bar Dimension (Wedge – I) (in mm)		
1	Length	10 mm
2	Width	8.5 mm
3	Thickness	2.5 mm

Table 9: Wedge - I dimensions (in mm)

Wedge Bar Dimension (Wedge – II) (in mm)		
1	Length	10 mm
2	Width	15 mm
3	Thickness	2.5 mm

Table 10: Wedge - II dimension (in mm)

Wedge bar (Wedge – II) has been used for the central domain of wing profile. On the edges the second wedge profile (Wedge I) has been used.

DSC Experimental Test

The test results of the DSC experimental test [2]

Transformation Temperatures	
Martensitic Finish Temperature	46.8 ^{O} C
Martensitic Start Temperature	56.7 ^{O} C
Austenitic Finish Temperature	69.4 ^{O} C
Austenitic Start Temperature	76.5 ^{O} C
Operating Temperature Range	46.8 ^{O} C - 76.5 ^{O} C

Table 11: DSC Experimentation

Solver Scheme: Joule Heating Study

Joule heating study is one of the integral working principals to simulate electrical actuation models for shape memory alloys.

Working Principal of Joule Heating Model:

$$LHS: \rho * A_c * C_P * \frac{d\theta}{dt}$$

$$RHS: i^2 * R - h_c * A_c[(T_{steady\ state} - T_{reference\ temp}$$

Results

In the results section, firstly the current density profile has been observed to understand and gauge the tendency of the bar to deform.

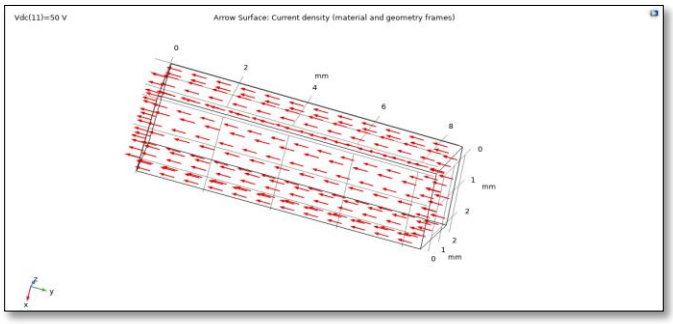

Figure 18 : Current Density Vector plot (At Maximum Voltage)

In the next results section, it is followed by studying directional displacement along the profile has been also observed to verify that the bar is able to actuate the wing.

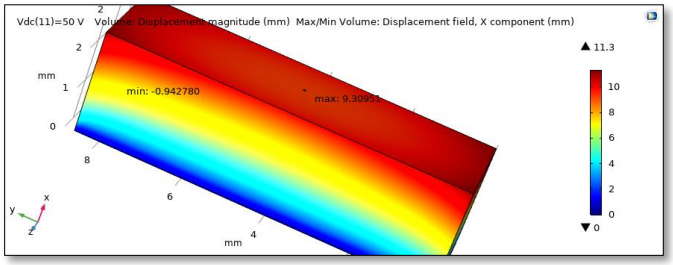

Figure 19 : Directional Displacement Study (At Maximum Voltage, V = 50V)

Principal Stress field study (Von Mises):

In the principal stress field study, the voltage is varied from 1 V to 50 V (Figure 18 – Figure 28) to observe the von mises stress along the geometry of the profile.

The post-processing presented below is carried out specifically for Wedge – I profile.

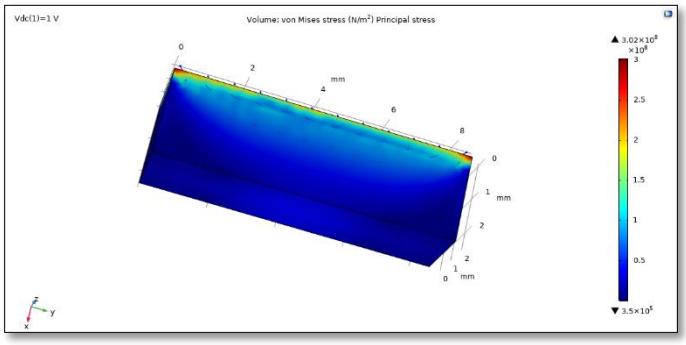

Figure 20: Von-misses Stress (Principal Stress study) (at V = 1V)

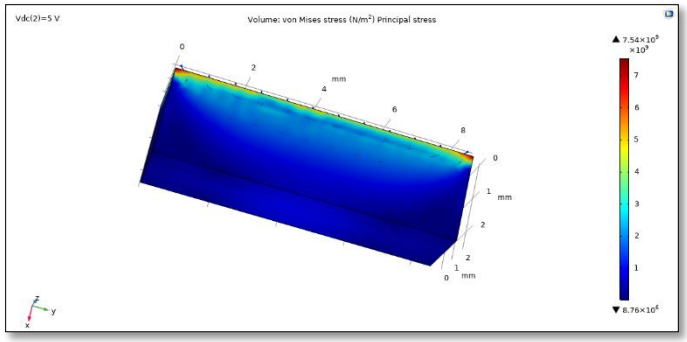

Figure 21: Von-misses Stress (Principal Stress study) (at V = 5V)

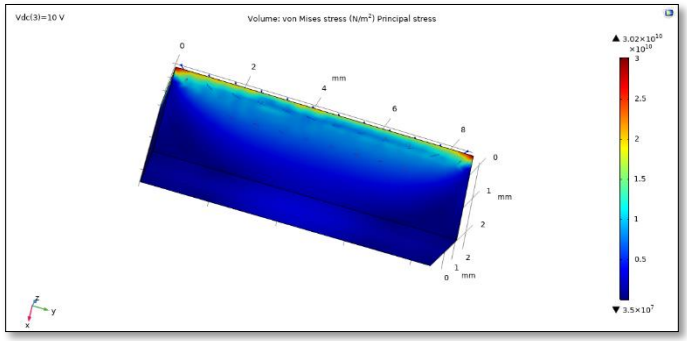

Figure 22: Von-misses Stress (Principal Stress study) (at V = 10V)

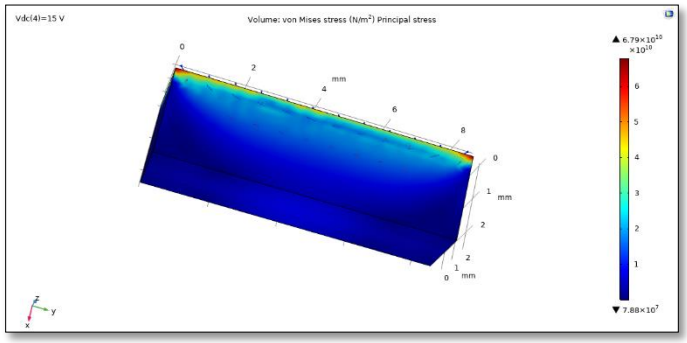

Figure 23: Von-misses Stress (Principal Stress study) (at V = 15V)

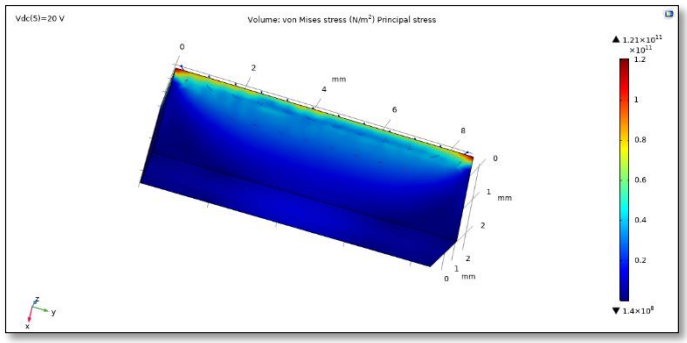

Figure 24: Von-misses Stress (Principal Stress study) (at V = 20V)

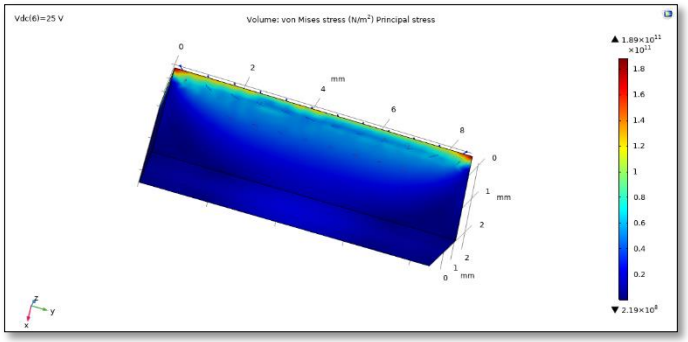

Figure 25: Von-misses Stress (Principal Stress study) (at V = 25V)

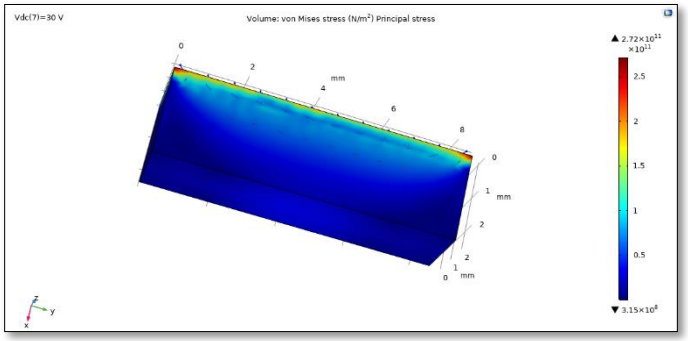

Figure 26: Von-misses Stress (Principal Stress study) (at V = 30V)

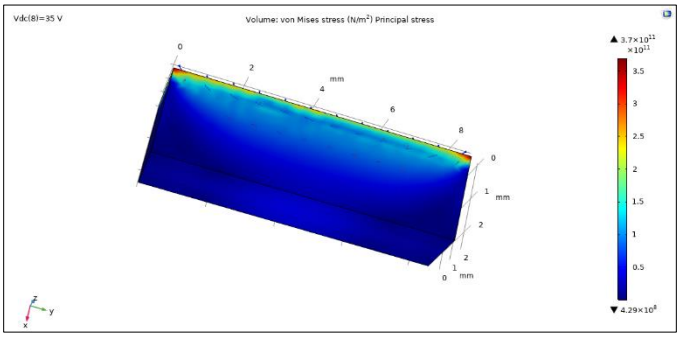

Figure 27: Von-misses Stress (Principal Stress study) (at V = 35V)

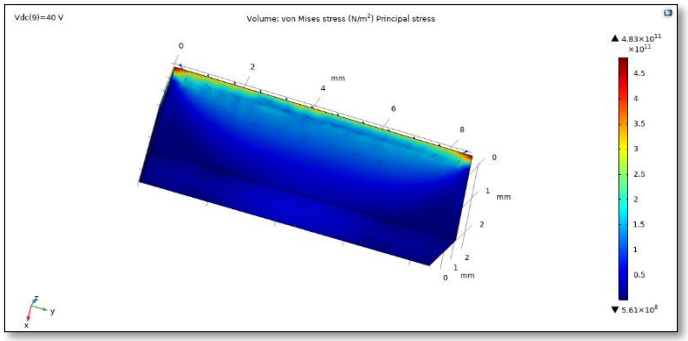

Figure 28: Von-misses Stress (Principal Stress study) (at V = 40V)

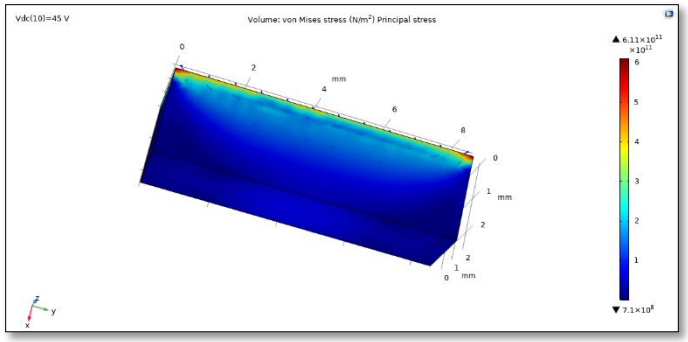

Figure 29: Von-misses Stress (Principal Stress study) (at V = 45V)

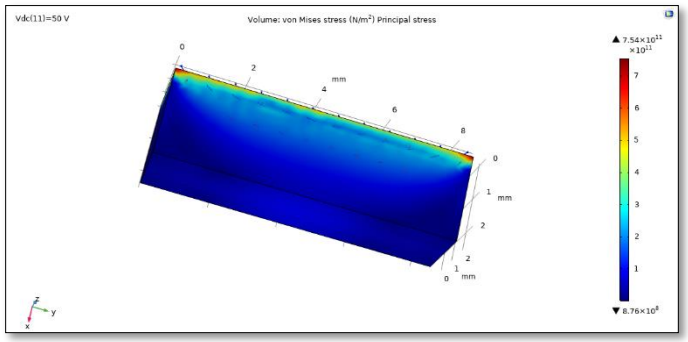

Figure 30: Von-misses Stress (Principal Stress study) (at V = 50V)

Principal Strain field study (Von Mises Strain):

In the principal strain field study, the voltage is varied from 1 V to 50 V (Figure 31 – Figure 40) to observe the von mises strain along the geometry of the profile.

The post-processing presented below is carried out specifically for Wedge – I profile.

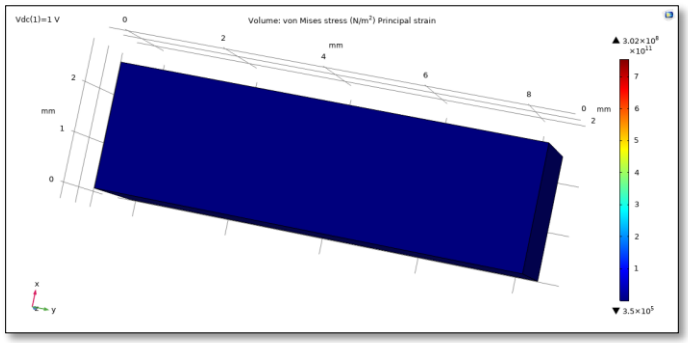

Figure 31: Von-misses Strain (Principal Strain study) (at V = 1V)

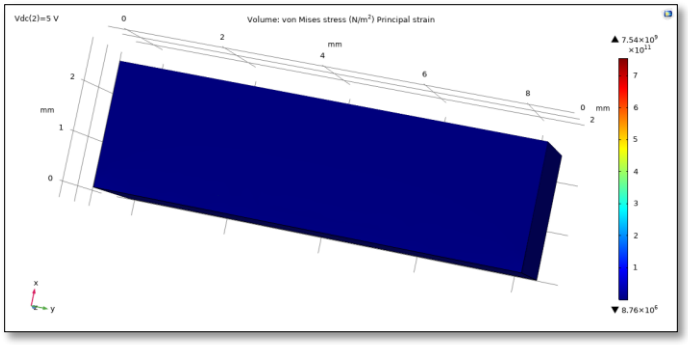

Figure 32: Von-misses Strain (Principal Strain study) (at V = 5V)

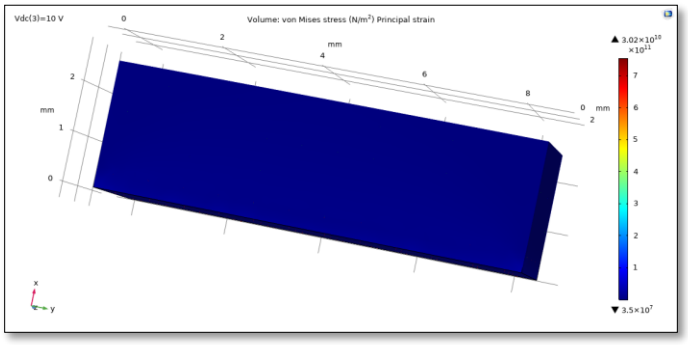

Figure 33: Von-misses Strain (Principal Strain study) (at V = 10V)

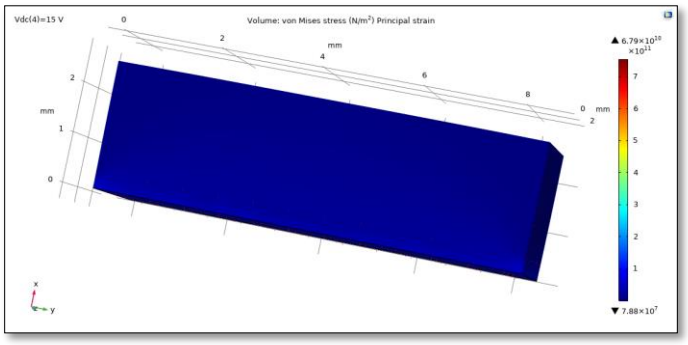

Figure 34: Von-misses Strain (Principal Strain study) (at V = 15V)

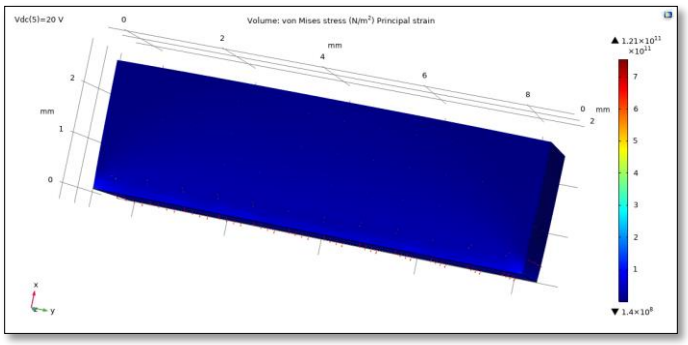

Figure 35: Von-misses Strain (Principal Strain study) (at V = 20V)

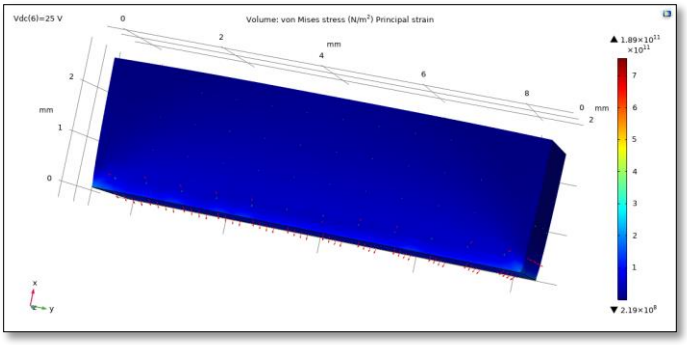

Figure 36: Von-misses Strain (Principal Strain study) (at V = 25V)

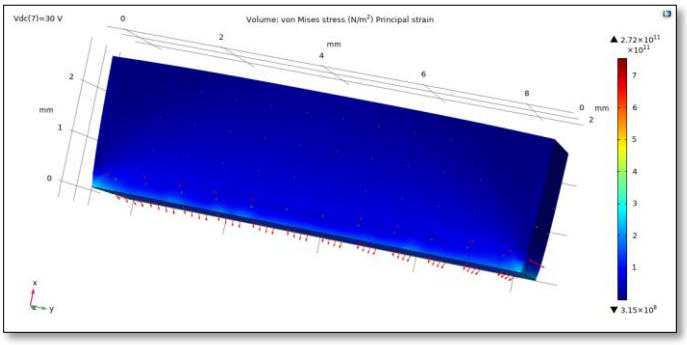

Figure 37: Von-misses Strain (Principal Strain study) (at V = 30V)

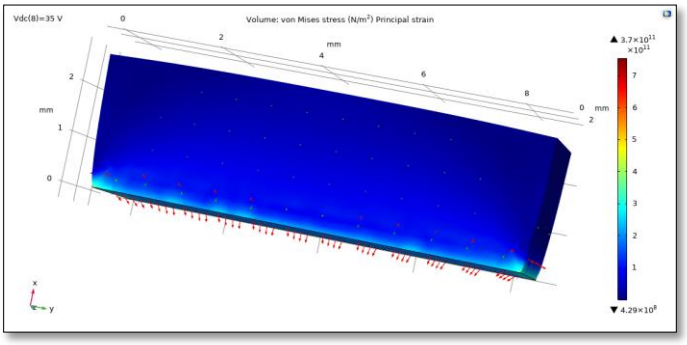

Figure 38: Von-misses Strain (Principal Strain study) (at V = 35V)

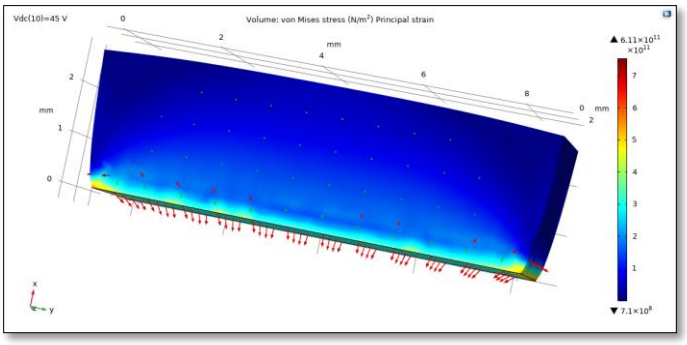

Figure 39: Von-misses Strain (Principal Strain study) (at V = 45V)

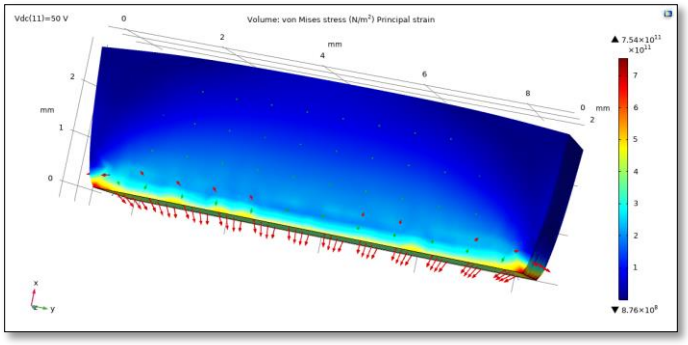

Figure 40: Von-misses Strain (Principal Strain study) (at V = 50V)

Parametric Study

In the given below parametric study, the voltage is iterated from 1V to 50V (Maximum Voltage) to study the displacements.

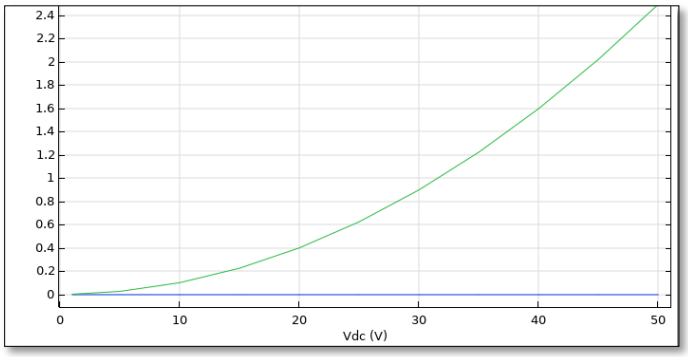

Figure 41: Parametric Study (Voltage - Displacement plot)

Inferences

By the above parametric study and our previously discussed fluid structural analysis, that the minimum voltage required to maintain the much-needed deflection should be more than 15 V with the current wedge bar profile serving as actuator to the wing.

On the structural aspects, the von mises stress and strain is well within the permissible design stress for the given load profile. Under the analysis scheme, even the thermal stresses have been also accounted.

Using the Joule Heating model for electrical actuation, the net resistance of the wedge can be calculated as follows:

Resistance Calculation (Wedge – I)	
Resistivity	76 Ω x 10^{-6} .cm
h_c	150 J/(m^2 . ^{O} C. sec)
Density (kg / m^3)	6460 kg / m^3
C_p	0.2 kcal /kg. ^{O} C
Area	25 x 10^{-6} m^2
Length	15 x 10^{-3} m
Resistance	2.58 x 10^{-2} Ω
Current (i)	2.41 A (at max V)

Table 12: Resistance Calculations for Wedge - I profile

Resistance Calculation (Wedge – II)	
Resistivity	76 Ω x 10^{-6} .cm
h_c	150 J/ (m^2 . ^{O} C. sec)
Density (kg / m^3)	6460 kg / m^3
C_p	0.2 kcal /kg. ^{O} C
Area	40 x 10^{-6} m^2
Length	8.5 x 10^{-3} m
Resistance	2.85 x 10^{-2} Ω
Current (i)	2.91 A (at max V)

Table 13: Resistance Calculation for Wedge - II profile

Now, as the above calculations were done for the modelled wedge. Now, practically the SMA can only be constructed using wire geometry. The wedges would be made out of combined SMA wires to model for the entire system. Now, the geometrically, its not the efficient model, but due to inability of thin sheet constructions out of SMA wire, this'll be closest approximation of the real time model.

In the last section of our discussion, system level calculations have been carried out to stipulate minimum current required for the system to operate. Whereas the resistance offered by the combination of wires stacked together for a given wedge would be modelled in series.

Overall, the system of wedges (wedge – I and wedge – II) are connected in parallel to calculate minimum current required for the entire system to actuate to stay as per the DSC experimental model.

Overall System Level Calculations		
1	Area of Cross Section (SMA Wire)	3.141 x 10^{-8} m^2
2.1	Area of Cross Section (Wedge – I)	25 x 10^{-6} m^2
2.2	Number of Wedge – I required	2(R) + 2(L)
2.3	Total Area (Combined Wedge)	100 x 10^{-6} m^2
2.4	Number of Wire units (in series for Wedge – I)	3183
2.5	Total Resistance (All Wedge – I) (in Series)	82.12 Ω
3.1	Area of Cross Section (Wedge – II)	40 x 10^{-6} m^2
3.2	Number of Wedge – II required	3
3.3	Total Area (Combined Wedge)	120 x 10^{-6} m^2
3.4	Number of Wire units (in series for Wedge – II)	3820
3.5	Total Resistance (All Wedge – II) (in Series)	90.71 Ω

4	Desired Final Temperature (Overall System Temperature)	70 ^{O} C
4	Total Resistance (Wedge – I + Wedge II) (in parallel)	43.1 Ω

Table 14: System level Calculation for Wedge – I and Wedge II connected in parallel

With the above set of calculations, with applied voltage V = 20V, the minimum net current requirement for the system to operate will be 464.037 mA with desired final temperature as 70 ^{O} C (steady state) to operate in the stipulated operating temperature range, as discussed in the earlier sections.

Future Scope of Research

In the future scope of research, the project can be studied with the aim to create non-linearized model of control to establish the actuation mechanism with control theory. At the same time ensuring the state-space representation could lead to achieving the controlled strain recovery for the entire system.

The controlled strain would further bolster the prospects of its utilization in commercial applications. Further, validation studies by physical prototype to simulate real-time conditions could serve as the starting point to lead further investigation in the dynamic analysis aspect of the current research.

References

1. U. Icardi, L. Ferrero, Preliminary study of an adaptive wing with shape memory alloy torsion actuators, Materials & Design, Volume 30, Issue 10, 2009, Pages 4200-4210.
2. H. Sayyaadi, M.R. Zakerzadeh, H. Salehi, A comparative analysis of some one-dimensional shape memory alloy constitutive models based on experimental tests, Scientia Iranica, Volume 19, Issue 2, 2012, Pages 249-257.
3. Cui, D., Song, G., and Li, H., "Modeling of the electrical resistance of shape memory alloy wires", Smart Material Structures, vol. 19, no. 5, 2010. doi:10.1088/0964-1726/19/5/055019.
4. Fareeq, Shelan. (2015). Aerodynamic evaluation of racing wings of a formula car.
5. Leo, D. J. (2007). In *Engineering analysis of smart material systems* (pp. 298–345). essay, John Wiley & Sons.
6. Marchesin, Felipe & Barbosa, Roberto & Gadola, Marco & Chindamo, Daniel. (2017). High downforce race car vertical dynamics: aerodynamic index. Vehicle System Dynamics. 56. 1269-1288.
7. Fonzi N. Brunton S. L.and Fasel U. 2020 Data-driven nonlinear aeroelastic models of morphing wings for control *Proc. R. Soc. A*.476: 20200079. 20200079. http://doi.org/10.1098/rspa.2020.0079
8. Stephen Daynes, Xavier Lachenal, Paul M. Weaver, Concept for morphing airfoil with zero torsional stiffness, Thin-Walled Structures, Volume 94, 2015, Pages 129-134, https://doi.org/10.1016/j.tws.2015.04.017.
9. Keshav Sharma, G. Srinivas, Flying smart: Smart materials used in aviation industry, Materials Today: Proceedings, Volume 27, Part 1, 2020, Pages 244-250, ISSN 2214-7853, https://doi.org/10.1016/j.matpr.2019.10.115.